IOPscience iopscience.iop.org

Home Search Collections Journals About Contact us My IOPscience

Preparation and morphological and optical characterization of azo-polymer-based SiO_2 sonogel hybrid composites

This article has been downloaded from IOPscience. Please scroll down to see the full text article.

2009 Smart Mater. Struct. 18 085024

(http://iopscience.iop.org/0964-1726/18/8/085024)

View the table of contents for this issue, or go to the journal homepage for more

Download details:
IP Address: 132.248.12.224
The article was downloaded on 19/01/2011 at 18:51

Please note that terms and conditions apply.

Smart Mater. Struct. **18** (2009) 085024 (14pp) doi:10.1088/0964-1726/18/8/085024

Preparation and morphological and optical characterization of azo-polymer-based SiO_2 sonogel hybrid composites

Omar G Morales-Saavedra[1,3], Fernando G Ontiveros-Barrera[1], Vicente Torres-Zúñiga[1], José Guadalupe-Bañuelos[1], Roberto Ortega-Martínez[1], Ernesto Rivera[2,3] and Tonatiuh García[2]

[1] Centro de Ciencias Aplicadas y Desarrollo Tecnológico, Universidad Nacional Autónoma de México, CCADET-UNAM, AP 70-186, Coyoacán, 04510, México, DF, Mexico
[2] Instituto de Investigaciones en Materiales, Universidad Nacional Autónoma de México, IIM-UNAM, AP 70-360, Coyoacán, 04510, México, DF, Mexico

E-mail: omar.morales@ccadet.unam.mx and riverage@iim.unam.mx

Received 15 January 2009
Published 23 July 2009
Online at stacks.iop.org/SMS/18/085024

Abstract
The well-established catalyst-free sonogel route was successfully implemented to fabricate highly pure, optically active, solid state polymeric azo-dye/SiO_2-based hybrid composites. Bulk samples exhibit controllable geometrical shapes and monolithic structure with variable dopant concentrations. Since the implemented azo-dye chromophores exhibit a push–pull structure, hybrid film samples were spin-coated on ITO-covered glass substrates; molecular alignment was then performed via electrical poling in order to explore the quadratic nonlinear optical performance of this kind of composite. Comprehensive morphological, spectroscopic and optical characterization of the samples were performed with several experimental techniques: atomic force microscopy, x-ray diffraction and infrared, Raman, photoluminescent and ultraviolet–visible spectroscopies. The linear refractive indices of both bulk and thin film samples were measured according to the Brewster angle technique and a numerical analysis of the transmission spectral data, respectively. Regardless of the low glass transition temperatures of the studied polymers, some hybrid film samples were able to display stable nonlinear optical activity such as second harmonic generation. Results show that the chromophores were satisfactorily embedded into the highly pure SiO_2 sonogel network without significant guest–host molecular interactions, thus preserving their optical properties and producing sol–gel hybrid glasses suitable for optical applications.

(Some figures in this article are in colour only in the electronic version)

1. Introduction

Azo-polymers have been considered as highly versatile materials due to the photoinduced motions occurring in them and their NLO properties [1]. Some reviews covering most of the implications of such materials have been published [1–4]. In recent years, various azo-polymers bearing amino–nitro-substituted azobenzene units have been synthesized and characterized [5]. In general, they have a maximum absorption wavelength close to that reported for similar push–pull azo-compounds [6, 7]. In these materials, both J-and H-type aggregation have been observed in cast films [5].

[3] Authors to whom any correspondence should be addressed.

 © 2009 IOP Publishing Ltd Printed in the UK

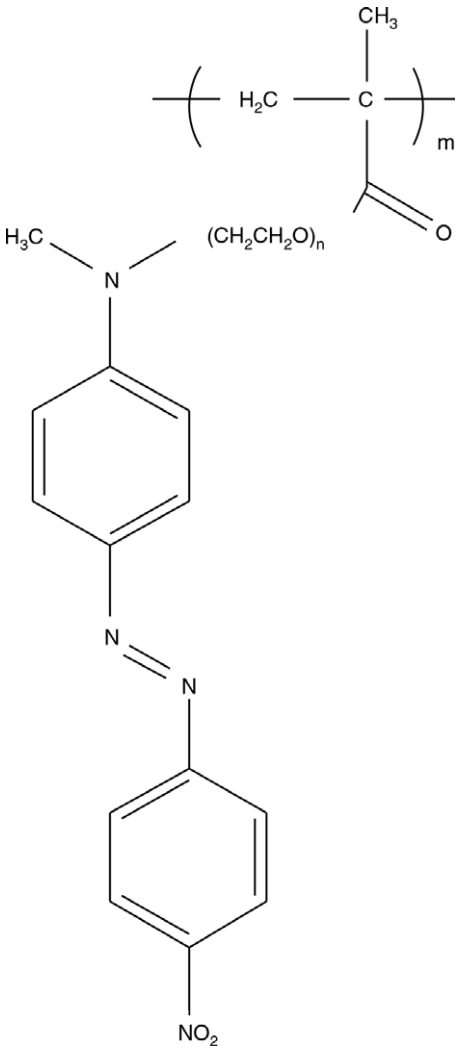

Figure 1. Chemical structures of the pMDR1 and p*n*PEGMAN polymers implemented as dopant species for sonogel networks.

Recently, we carried out the synthesis and characterization of a novel series of azo-polymers bearing well-defined oligo(ethylene glycol) spacers, called p*n*PEGMAN [8]. According to this nomenclature, p means polymer, n indicates the number of ethylene glycol units in the spacer, PEG indicates the presence of a short poly(ethylene glycol) segment, M means methacrylate and AN indicates the presence of an amino–nitro-substituted azobenzene. Four different p*n*PEGMAN polymers with $n = 2$, 3, 4 and 6 were synthesized. A model polymer containing dispersed Red-1 units (pMDR-1) was also prepared to be used as a reference according to the method reported in the literature [8, 9]. The structure of the p*n*PEGMAN polymers is shown in figure 1.

In this paper, we report on the preparation of SiO_2-based solid state hybrid p*n*PEGMAN and pMDR1 materials in both thin film and bulk samples by the catalyst-free (CF) sonogel route. Both the thin film and bulk sol–gel sample formats offer important possibilities for the development of several high-tech photonic and optoelectronic applications. Hence numerous optical and nonlinear optical (NLO) studies were selectively carried out on these samples: optical characterizations were performed on thin film and bulk samples in order to determine important optical parameters (absorption and emission bands and linear refractive indices). NLO measurements include the test of the hybrid thin films deposited on glass substrates covered with ITO (indium tin oxide) film electrodes for electrical poling of the guest molecular systems in order to explore their quadratic NLO performance according to the second harmonic generation (SHG) technique. On the other hand, x-ray diffraction (XRD), Raman and FTIR spectroscopy studies were sequentially performed in order to explore possible interactions between the host SiO_2 matrix and the guest polymers. These hybrid materials may provide practical alternatives to expensive inorganic monocrystalline materials, for instance, in the development of linear and nonlinear organic–inorganic photonic prototypes.

Table 1. Glass temperature transitions (T_g values) and calculated dipole moments (μ values, calculated from a model using the semi-empirical method PM3) for the pMDR1 and p*n*PEGMAN azo-polymers.

Polymer guest sample	T_g values (°C)	Dipole moment μ values (D)
pMDR1	13.12	6.2
P2PEGMAN	41.77	6.5
P3PEGMAN	20	6.45
P4PEGMAN	27	6.68
P6PEGMAN	31	6.33

2. Experimental details

2.1. Preparation of SiO_2-based catalyst-free sonogels as host network for pMDR1 and pnPEGMAN azo-polymers

The preparation of the *nPEGMAN* monomers and the p*n*PEGMAN polymers has been recently carried out [8, 9]. Since these polymers contain (push–pull) amino–nitro-substituted azobenzenes, they display a high dipole moment value as well as a non-centrosymmetric molecular structure which makes them good prospects to obtain materials with optical and NLO properties. Table 1 shows the calculated dipole moments (μ values, calculated from a model using the semi-empirical method PM3) and the glass temperature transitions (T_g values) for the pMDR1 and p*n*PEGMAN polymers; although with relatively low T_g values, the sonogel environment has been demonstrated to preserve the optical properties and to increase the thermal stability of the embedded organics [10, 11], which makes the new p*n*PEGMAN polymers interesting candidates to be tested within the sonogel network in order to study their NLO performance.

The sol–gel method has been frequently used to synthesize amorphous SiO_2 based on the hydrolysis of different precursors such as TEOS, TMOS, etc, followed by condensation reactions of the hydrolyzed species [12]. This methodology has been widely adopted as a suitable way to obtain glassy doped materials with good optical and mechanical qualities. Both hydrolysis and condensation reactions occur normally in the presence of acidic or basic catalysts where ethanol or methanol are commonly used as

standard solvents for the precursor and water reactants. In this work, a different approach for the preparation of highly pure SiO_2 sol–gel (sonogel) materials is exploited. In this case, the use of both solvents and catalysts is fully suppressed and the hydrolyzed species are substituted by molecular radicals generated by ultrasound. Extensive details on the synthesis, chemistry and methodology to produce these novel materials have been given in the literature [11, 13]. In the present paper, the catalyst-free sonogel route was successfully implemented to obtain SiO_2 networks with high optical quality as host materials for the recently synthesized azo-polymers. Following a well-established procedure recently proposed [11, 13], a precursor solution of 25 ml of tetraethyl-orthosilicate (TEOS, Fluka 99% purity) and 25 ml of distilled water were mixed in a glass vessel and stabilized at 1 °C for 1 h before ultrasonic (US) irradiation. A metallic ultrasound tip (Cole-Parmer-CPX, 1.25 cm in diameter), carefully located at the TEOS/H_2O surface interface, provides an effective irradiation power density of the order of 3.2 W cm^{-3} at 20 kHz. The tip of the ultrasonic-wave generator also acts as an ultrasonic homogenizer. After 3 h of programmed US irradiation (on/off intermittent sequences of 5 s, net irradiation time: 1.5 h), the sonicated suspension was kept in the reactor vessel at room conditions for about 24 h; thereafter two immiscible phases appear: the upper one, corresponding to unreacted TEOS, was removed and eliminated, whereas the lower phase corresponding to a stable colloidal suspension and containing the sonicated induced hydrolyzed product (OH-TEOS) was carefully dropped into cylindrical Teflon containers at different volumes. The pMDR1 and p*n*PEGMAN compounds, previously dissolved in tetrahydrofuran (THF), were afterwards added and ultrasonically mixed with the deposited colloidal suspensions in order to start the inclusion of dopants within the CF-SiO_2 matrix and the formation of bulk hybrid composites or thin film samples via a home-made spin-coating system.

In the present application, dopant dissolutions (D-D) containing 30 mg of the studied compounds and 10 ml of THF solvent were prepared (3 mg ml^{-1}). The molecular materials showed good solubility in THF, thus saturated solutions were ensured in order to fabricate several highly loaded, optically active sonogel composites. For bulk monolithic hybrids, the dose ratio of the OH-TEOS versus the dopant dissolution (OH-TEOS:D-D) was carefully prepared with a precise volumetric micropipette and deposited into the cylindrical Teflon containers (1 inch in diameter, 2 ml in volume) in order to obtain different doped optical glasses. The prepared hybrid materials at high dopant concentrations were generated according to the previous methodology with a starting total volume of 2 ml, varying the OH-TEOS:D-D concentration ratio (in volume) as follows: 1.0:1.0, 1.2:0.8, 1.4:0.6, 1.5:0.5, 1.6:0.4 and 1.8:0.2 ml. Extremely low doped samples were also fabricated with these polymers with a starting solution of 1.8 mg ml^{-1} and the following concentrations: 1.90:0.02 and 1.90:0.05 ml. Undoped or pure reference (PR)-sonogel samples (2.0:0.0) were also prepared for reference and calibration purposes. The samples were isolated while drying with a plastic cover in order to avoid atmosphere and temperature variations, and conserved for two to three weeks at room conditions in closed vessels with a small hole in the cap in a clean–dry–dark environment. Rigid and geometrical monoliths adequate for optical characterization were obtained after this slow drying process. The resulting bulk hybrids possess higher purity compared to other traditionally synthesized sol–gel hybrid composites, because the use of the US waves instead of reactive solvents and catalyst gives samples with higher optical quality [11, 13]. The bulk samples, generally obtained for very slow drying speeds, showed monolithic cylindrical shapes with diameters and thicknesses varying from 7 to 10 mm and 0.7 to 1.4 mm, respectively. In fact, according to previously published reports [11, 14, 15], solutions of organic dopants in THF are better incorporated into the CF-sonogel network, since the S_4 geometry of TEOS implies a zero dipolar moment and would not accept the inclusion of highly polar THF-based solutions. The OH-TEOS group is, in contrast, highly polar and provides an optimal environment for molecules dissolved in THF.

For thin film sample preparation, D-D of the polymers in THF were prepared with 7.6 mg ml^{-1}, then ultrasonically mixed with the OH-TEOS at a per cent ratio of 50/50%; ITO-coated glass substrates from Sigma-Aldrich (cat. no. 576352-25) were spin-coated with 1 ml of the OH-TEOS/D-D mixtures for 5 s at a constant speed of 1.5×10^3 rpm. Homogeneous film depositions, suitable for optical characterization, were obtained under these conditions.

2.2. Optical and structural characterization of hybrid pMDR1-and pnPEGMAN-based SiO_2 sonogel networks

2.2.1. Spectroscopic measurements. Bulk and thin film hybrid samples were analyzed by UV–vis absorption spectroscopy within the 200–1100 nm spectral range using the double-beam Shimadzu-260 UV–vis spectrophotometer. Spectra were compared to those obtained from the same compounds in non-saturated THF solutions in order to ensure that the Beer–Lambert law applies for such slightly loaded (partially transparent) solutions; in this way the induced band shifts produced by the sol–gel confinement were carefully detected. Photoluminescent (PL) measurements were obtained for bulk samples in the 300–900 nm spectral range with the FluoroMax-3, Jobin-Yvon-Horiba fluorimeter. The excitation wavelengths were selected according to the UV–vis absorption spectra of the liquid or solid state hybrid samples at a convenient wavelength (near the absorption wavelength maximum or at optimal excitation/emission conditions). Such UV–vis and PL studies were initially carried out in order to verify the inclusion of the guest molecular systems within the SiO_2 porous network and the optical quality of the samples, but also to provide preliminary information concerning the electronic properties of these materials for optical and nonlinear optical applications. FTIR spectra of the bulk samples were recorded in prepared KBr pellets (at 1 wt% concentration of the 1.2:0.8 hybrid samples) with a Thermo-Nicolet Nexus 670 FTIR spectrometer within the 400–400 cm^{-1} spectral range. An Almega-XR dispersive Raman

spectrometer equipped with an Olympus microscope (BX51) was used to obtain the Raman spectra of the bulk hybrid samples. An Olympus 50× objective lens (NA = 0.45) was used as the focusing optical system for the Raman laser source; the spot size of the focused laser beam on the sample was ∼1.5 μm^2. The same objective was also implemented as the collecting optical system for the backscattered light in a 180° backscattering configuration. The scattered light was detected by a charge-coupled device (CCD) detector, thermoelectrically cooled to −50 °C. The spectrometer used a convenient optical grating (675 lines mm^{-1}) to resolve the scattered radiation and a notch filter to block the Rayleigh light. The pinhole of the monochromator was set at 25 μm and the Raman spectra were integrated over 20 s with a resolution better than 4 cm^{-1}. The excitation source was obtained from a Nd:YVO_4 laser (frequency doubled at 532 nm) and the incident power at the sample was ∼8 mW. Both FTIR and Raman measurements were performed at atmospheric pressure of 560 Torr and room temperature.

2.2.2. Linear refractive index measurements. The evaluation of the linear refractive index of the bulk hybrids was carried out using an unpolarized He–Ne laser system ($\lambda = 632$ nm) according to the Brewster angle methodology. At this incident angle, only the perpendicular (S) component of the laser source is reflected on the surface of the monolith, thus the intensity of this beam becomes a minimum. From this effect, the linear refractive index can be estimated according to the following relation: $n_t/n_i = \tan\psi$, where $n_i = 1$ (air) and n_t is the refractive index of the hybrid sample, whereas ψ represents the Brewster angle. Refractive indices of the hybrid films were indirectly measured by numerical processing of the data obtained from the optical transmission spectra of the samples (implementing the envelope method [16–18]). This is a reliable procedure commonly used in semitransparent thin films as a low-cost alternative to ellipsometric spectroscopy (ES), which consists of the analysis of typical interference fringes produced in the transmission spectra within a wide spectral range. The refractive indices (discrete dispersion curves) of the films were calculated using this methodology on the basis of the following physical approach [17]:

$$n_{\mathrm{Film}} = [N + (N^2 - n_S^2)^{1/2}]^{1/2}, \tag{1}$$

$$N = 2n_S\left[\frac{1}{T_{\min}} - \frac{1}{T_{\max}}\right] + \frac{n_S^2 + 1}{2}, \tag{2}$$

where $T_{\max}$ and $T_{\min}$ correspond to measured and interpolated points lying between the two envelope curves at maxima and minima of the transmittance intensities and found at certain wavelengths λ_i and n_S is the refractive index of the respective glass substrate. Since the envelope method is able to predict discrete values of the refractive indices at the corresponding λ_is, the continuous dispersion curve can be further obtained implementing a Cauchy function of the form $n_{\mathrm{Film}}(\lambda) = a + b/\lambda + c/\lambda^2$ (where λ is the wavelength and a, b, and c are constants related to the structure and composition of the material); this is possible as the experimental values of the refractive index of the film samples are found to nearly fit this kind of relation [19].

In addition, the envelope method also permits the estimation of the film thickness d. This parameter was also calculated using the following relation [18]:

$$d = \frac{M\lambda_1\lambda_2}{n_{\mathrm{Film}}(\lambda_1)\lambda_2 - n_{\mathrm{Film}}(\lambda_2)\lambda_1}, \tag{3}$$

where M is the number of oscillations between two selected maxima or minima points ($M = 1$ for two consecutive maxima or minima); $n(\lambda_1)$ and $n(\lambda_2)$ are the refractive indices at the corresponding selected maxima/minima points at λ_1 and λ_2. Thus a given M number of d values can be obtained and the respective average (d_{ave}) can be further used to iteratively improve this value by implementing the following formula, again taking into account the transmission interference fringes:

$$2n_{\mathrm{Film}}d_{\mathrm{ave}} = m\lambda, \tag{4}$$

where m takes the value of an integer for a maximum, and a half-integer for a minimum. Using d_{ave}, m can be obtained from equation (4); this value is rounded off to the nearest integer for a maximum, or half-integer for a minimum, in order to obtain the modified m' value. Now again, from equation (4), given the m', λ and n_{Film} parameters, a set of more accurate d' values can be obtained. The average d'_{ave} value is reported as a representative thickness of the hybrid films, which can then be compared to AFM measurements. All numerical routines implementing the envelope method were programmed in MatLab v. 6.

2.2.3. NLO–SHG measurements. The hybrid thin films were studied as active media for quadratic $\chi^{(2)}$-nonlinear optical effects such as SHG. Measurements were performed after electrical poling of the samples via a corona-poling system working at 6.5 kV (working distance of the needle: 1.5 cm). The implemented SHG experimental set-up consists of a commercial Q-switched Nd:YAG laser system (Surelite II from Continuum, $\lambda_\omega = 1064$ nm, repetition rate of 10 Hz and a pulse width of $\tau \approx 22$ ns) which was implemented to provide the fundamental wave. Pulse powers were filtered in order to avoid any thermal damage on the samples. The polarization of the fundamental beam (S or P polarizing geometry) was selected by means of an IR-coated Glan-Laser polarizer and a $\lambda/2$ quartz retarder. A second polarizer was used as the analyzer allowing the characterization of the SHG signals. The second harmonic waves (at $\lambda_{2\omega} = 532$ nm) were detected by a sensitive photomultiplier tube placed behind interferential optical filters (centered at 532 ± 5 nm). The SHG device was calibrated by means of a Y-cut α-quartz crystal, wedged in the d_{11} direction ($d_{11} = 0.64$ pm V^{-1}), which is commonly used as a NLO reference standard via the Maker–Fringes method [20–23].

2.2.4. XRD spectra. The structure of the hybrid composites was determined through x-ray diffraction by the θ–2θ technique on a Brucker D8 Advance diffractometer using the Cu Kα_1 ($\lambda = 0.154\,05$ nm) radiation.

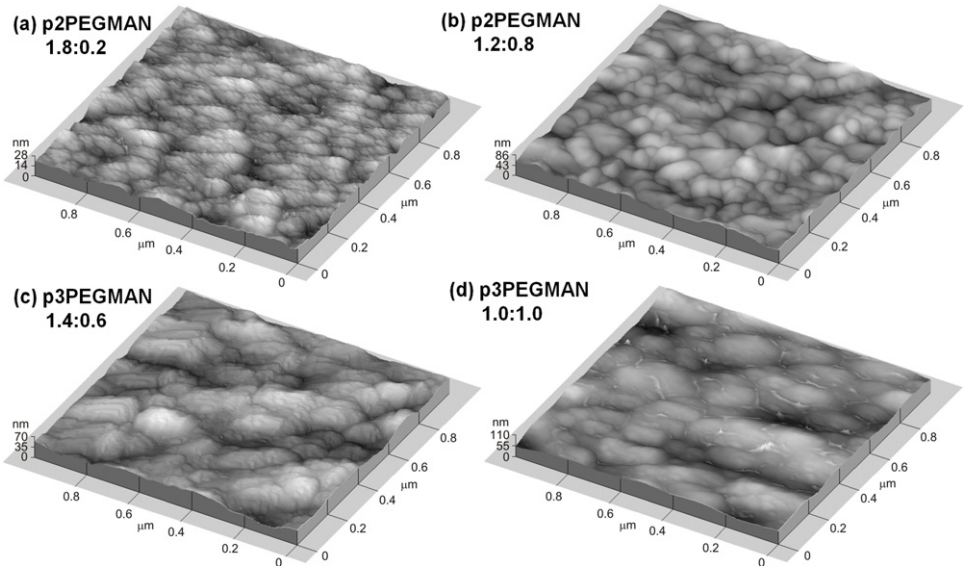

Figure 2. 3D micrographs obtained by AFM, showing the surface morphology of selected bulk hybrid samples for increasing dopant concentrations: (a), (b) p2PEGMAN-based hybrids with 1.8:0.2 and 1.2:0.8 concentrations, respectively, (c), (d) p3PEGMAN-based hybrids with 1.4:0.6 and 1.0:1.0 concentrations, respectively.

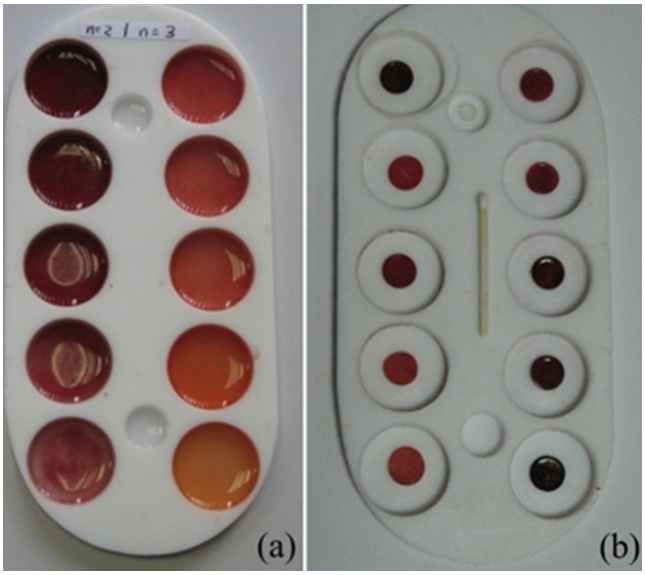

Picture 1. Fabrication procedure of the sonogel hybrid composites: (a) Teflon containers filled with a mixture of a pMDR1 and p*n*PEGMAN-based THF solution and the H-TEOS (red colored liquid mixtures in sol phase). (b) After a few weeks, the drying process is concluded and the shrinking process takes place due to slow dehydration and polymerization of the p*n*PEGMAN–pMDR1/THF/H-TEOS mixtures to form the SiO_2-doped networks; some of the samples crack at this stage. In this picture, selected heavily and slightly doped pMDR1 and p*n*PEGMAN-based hybrid monolithic glasses are shown, where the geometric shape is conserved (a transparent, undoped reference sample is shown in one of the smaller Teflon containers).

2.2.5. AFM morphology. The surface morphology of bulk and film samples and thickness of the films were studied by atomic force microscopy (Park AutoProbe CP equipment); the acquisition of images was performed in contact mode with an interaction force applied between the sample and the AFM tip of 1.0 nN. The AFM system was equipped with an SiN sharpened Microlever™ tip with typical force constant of 0.05 N m^{-1} and resonant frequency of 22 kHz which specify the mechanical characteristics of the cantilever used (typical constants of the instrument).

3. Results and discussions

3.1. AFM- and XRD-structural characterization

The set of pictures 1 shows results of the sonogel drying process for selected red colored p*n*PEGMAN-based hybrid samples; here, the initially filled Teflon containers exemplify, after a few days, the shrinking process due to dehydration. Samples are very susceptible to fractures if the environmental conditions are not favorable. However, after several weeks of ageing, once the drying course is fully completed under optimal environmental conditions, monolithic samples with geometrical shapes can be obtained with about 70–80% efficiency.

Surface morphology and the chromophore loading mechanical stability of some bulk sonogel and thin film hybrids were studied by high resolution AFM measurements. For this purpose, figure 2 shows several AFM micrographs of the morphology and structural dependence of the bulk hybrids with increasing dopant concentrations; here, high and low doped p*n*PEGMAN and pMDR1-based monoliths were selected for surface analysis. Bulk hybrid composites exhibit a stable and uniform texture with a homogeneous grain size distribution. As an example, figure 2 shows the AFM micrographs of low and high doped p*n*PEGMAN hybrids (1.8:0.2, 1.2:0.8 for $n = 2$, and 1.4:0.6, 1.0:1.0 for $n = 3$, respectively), revealing a remarkable enlargement of the average grain size distribution for increasing dopant concentrations. The texture of these

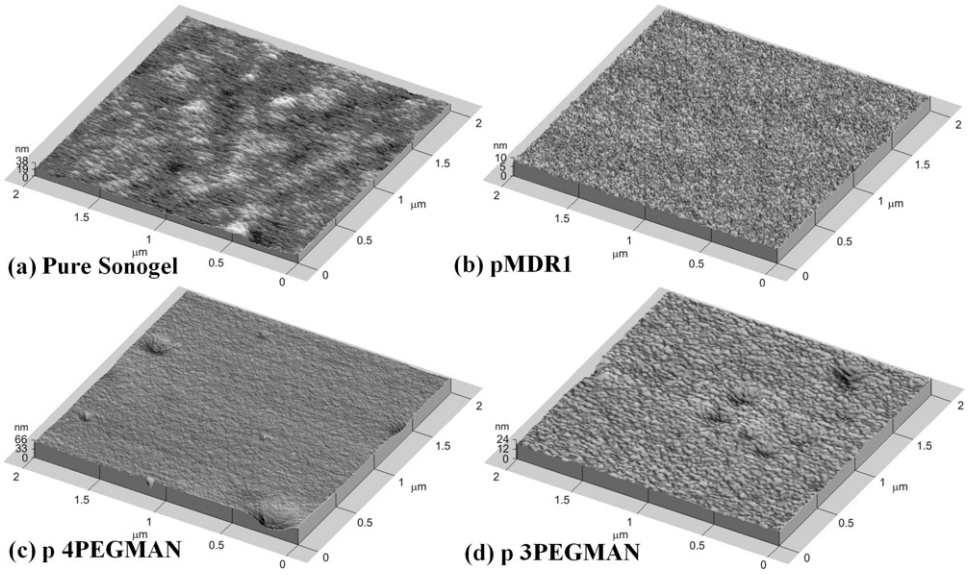

Figure 3. 3D micrographs obtained by AFM, showing the surface morphology of thin films deposited on Corning 7059 glass slices from: (a) the reference sonogel sample, (b) pMDR1-based hybrid film, (c) p4PEGMAN-based hybrid film and (d) p3PEGMAN-based hybrid film.

samples remains uniform in size and homogeneous without significant irregularities; however, an excessive chromophore loading leads to the deformation of the grain arrangements, resulting in more irregular textures which exhibit a rather disordered structure. All this may eventually lead to mechanically unstable structure configurations and to the rupture of the monolithic arrangement, as has been repeatedly confirmed for several highly loaded hybrids after drying. In fact, molecular segregation of the dopant chromophore solutions within the forming SiO_2 network takes place and the mechanical stability of the samples can be broken due to inner inter-pore strain caused throughout the shrinking process. We argue from a qualitative analysis that a most favorable pore size within the SiO_2 matrix should be achieved after the drying time, in which an optimal dopant concentration can be contained in order to support the mechanical strength of the SiO_2 network. As the dopant agent is increasingly added to the SiO_2 host matrix, a moderate enlargement of the constituting hybrid particles is observed. If an excessive overload of the dopant dissolution occurs, the solubility limit of the dopants within the gel phase is then overcome, phase segregation takes place and the dopant molecules are randomly dispersed among SiO_2 particles. As a consequence, a chaotic collapse of the sample occurs while drying, becoming highly unstable and the mechanical stability disappears to produce a fragile network. Nonetheless, high quality bulk optical samples with adequate mechanical strength can be obtained within the doping concentrations implemented in this work.

According to the previous observations, thin film samples with adequate OH-TEOS:D-D concentrations were prepared in order to ensure the best mechanical performance for optical characterization. In fact, as shown in figure 3 the spin-coated depositions of the pMDR1 and the p*n*PEGMAN-based hybrids (including the reference sonogel), exhibit, from amplified high quality digitized images (2 μm $\times$ 2 μm resolution), adequate surface morphology for optical characterization: all surfaces are, in general, homogeneously covered by grains with a narrow nanometric grain size distribution, showing structures of rounded or almost rod-shaped geometry. Uniform and regular surfaces with low inter-grain porosity (except for some defects detected in the $n = 3$ and 4 samples) and quasi-monomodal grain size distributions can be observed everywhere. The undoped sonogel deposition (rod-shaped geometry, see figure 3(a)) considerably differs from that of the hybrid films: noticeable structural changes are due to the higher viscosity of the pure sonogel (sol phase), which provokes an oriented particle organization along the centrifugal spin-coating direction.

On the other hand, as shown in figure 4, XRD patterns taken at room temperature on the bulk hybrids and reference sonogel sample exhibit, as expected, an amorphous organization certified by a broad peak detected in all measurements[4]. In fact, for the pure reference sonogel, this peak is centered at 25.37° which is characteristic of an amorphous silicon oxide phase [12, 13]. The XRD patterns of the doped composites show similar (in shape) amorphous curves to those observed for the reference sample, so that the hybrid composites remain as an amorphous/glassy phase. However, a noticeable shift of the XRD peak occurs for the patterns corresponding to the hybrid samples, namely to 22.7°, which indicates an effective structural change and the successful inclusion of the guest molecular systems. This effect may also be indicative, but not necessarily, of molecular interactions between the host network and the guest molecular systems (see section 3.2).

[4] As reported in the literature [13], the thermal evolution of the sonogel XR diffractograms show that the SiO_2 network undergoes crystalline phase transformations at higher temperatures: between 800 and 1200 °C broad bands corresponding to a mixture of tridymite and cristobalite can be observed; beyond 1200 °C the highly crystalline β-cristobalite phase takes place (optimally observed for samples treated at 1400 °C).

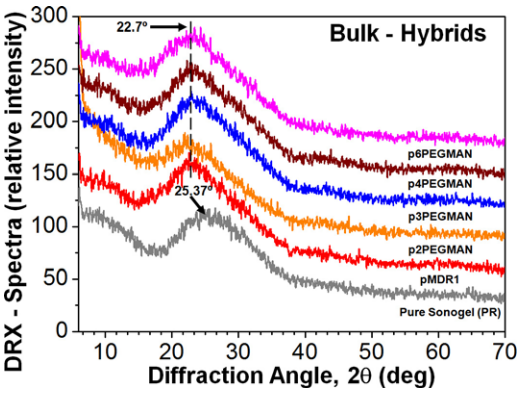

Figure 4. Comparative XRD spectra of the sonogel bulk hybrid composites and the reference sample.

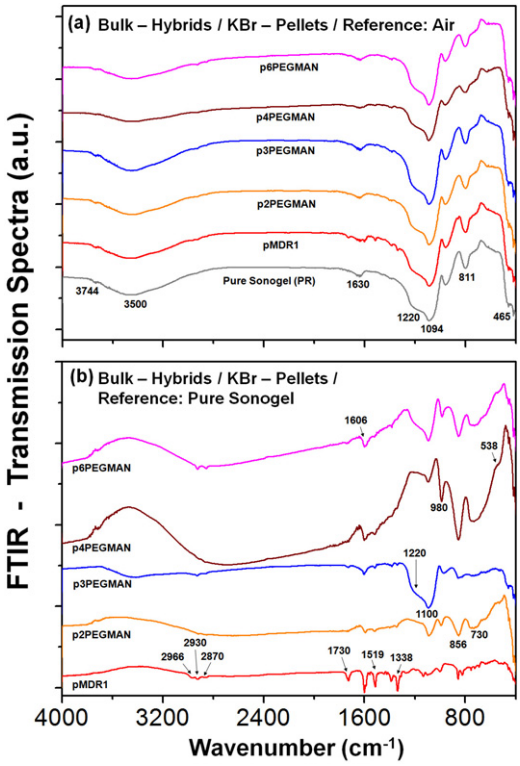

Figure 5. Comparative FTIR spectra of the bulk sonogel hybrid composites and the reference sample: (a) hybrid sol–gel material: sonogel SiO_2 matrix + polymer and (b) subtracting the spectrum of the pure sonogel network.

3.2. Overall spectroscopic and optical characterizations

According to section 3.1, FTIR and Raman spectra of the bulk hybrid samples were recorded at room conditions in order to explore any molecular interactions between the host network and the guest molecular system with the available spectroscopic techniques. FTIR spectra of the pristine p*n*PEGMAN polymers were recorded in KBr pressed pellets and shown to be practically identical since they have the same functional groups (spectra not shown here). The principal bands are listed: IR (KBr): 3100 (s, C–H aromatic), 2960 (CH_2), 2871 (s, CH_2 and CH_3), 1726 (C=O), 1601 (s, NO_2), 1517 (s, C=C aromatic), 1376 (s, N=N), 1336 (s, C–O ester), 1269 (C–N), 1100 (s, all O–CH_2), 858 (=C–H aromatic, out-of-plane) cm^{-1}. The main difference is the intensity of the band at 1100 cm^{-1}, which is due to all the OCH_2 groups present in the oligo(ethylene glycol) spacers within the polymers. This band is more intense, as the length of such spacers increases; in other words, this band has the highest intensity for p6PEGMAN and the lowest for p2PEGMAN.

FTIR spectra of the sonogel pMDR1 and p*n*PEGMAN-based hybrids, together with the corrected FTIR spectra subtracting the signals due to the pure sonogel network, are shown in figures 5(a) and (b), respectively (measurements were performed in KBr pressed pellets at 1% hybrid concentration). Figure 5(a) shows the infrared spectra at the Si–O vibration region of the gels, the overall vibrations corresponding to those expected for SiO_2-based sol–gel materials [12, 13]: (a) a strong and complex band at 1094 cm^{-1} with a shoulder at ∼1220 cm^{-1} is related to the asymmetric stretching vibration of the Si–O–Si bonds, bridging the SiO_4 structural units; (b) the band at 811 cm^{-1} corresponds to the symmetric stretching vibration of the Si–O–Si network, whereas the band at 465 cm^{-1} is assigned to the bending mode of the same bonds. Within the hydroxyl region of the dried gels, the small band at 3744 cm^{-1} corresponds to the terminal silanol groups and the wider bands centered at ∼3500 cm^{-1} are associated with hydroxyl groups from internal silanol, as well as residual water [12, 13, 24]. Finally, the band at 1630 cm^{-1} probably corresponds to the overtone of the strong absorption band assigned to the different SiO_4 unit vibrating modes. By contrast, the FTIR spectra subtracting the signals of the pure sonogel matrix (figure 5(b)) show a series of low intensity signals due to some of the functional groups present in the dopant molecular systems. For instance, the slightly shifted signals at 2930 cm^{-1} (s, CH_2 and CH_3), 2870 and 2966 cm^{-1} correspond to the symmetric and asymmetric compressions of the CH_3 molecular bonds, respectively [24]. 1730 (C=O), 1606 (C=C, doubtless superimposed on asymmetric stretching vibrations of NO_2), 1220 (s, C–O ester), 1100 (s, all O–CH_2), 980 (C=CH_3 rocking), 856 (=C–H aromatic, out-of-plane) cm^{-1} confirm the presence of the doping molecules within the sonogel matrix [24]; 730 cm^{-1} (NO_2), with the corresponding symmetric and asymmetric compressions (1342, 1519 cm^{-1}, respectively) and a 538 cm^{-1} band indicate molecular in-plane bending vibrations [24]. Some signals due to certain functional groups, which give less intense signals, could not be observed because of dilution.

Raman spectra of the pMDR1 and p*n*PEGMAN dopant polymers in THF solutions and derived bulk hybrids were obtained after focusing the incident laser beam onto the samples through the microscope objective as shown in figures 6(a)–(d). No major degradation of the samples was observed. The spectra of the THF solutions at ∼2 mg ml^{-1} concentration (see figure 6(a)) reveal some high, medium or low intensity bands within the 800–1700 cm^{-1} interval; these bands are mainly due to the modes of the different molecular functional groups. The Raman signal of THF is negligible within the whole spectral range, demonstrating optimal conditions for Raman measurements in this particular

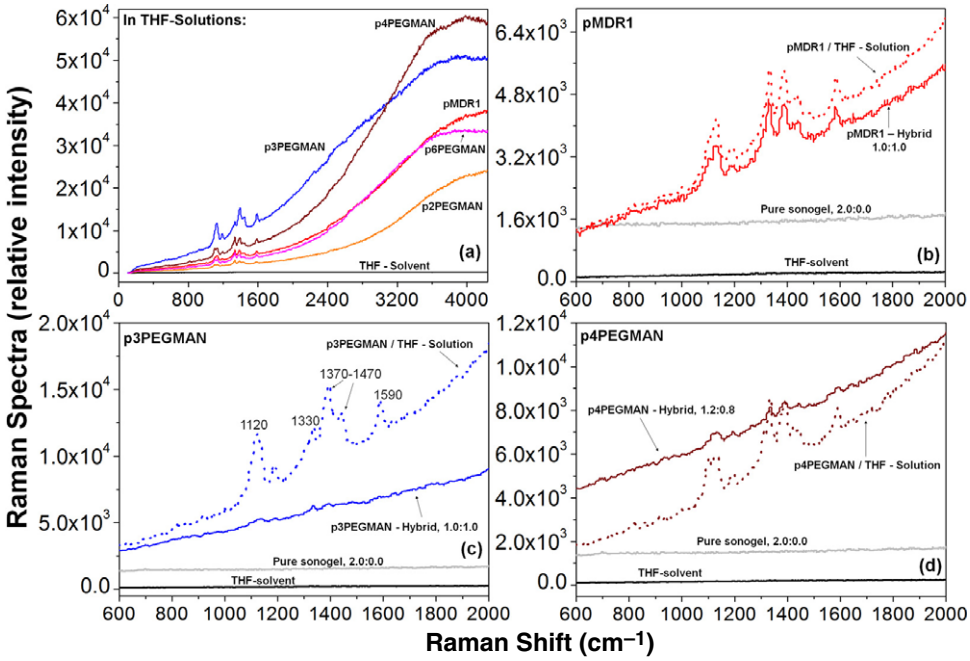

Figure 6. Comparative Raman spectra of the pMDR1 and p*n*PEGMAN polymers in THF solution and in solid state sonogel phases: (a) polymers in THF solutions, (b) spectra of pMDR1 in various environments, (c) spectra of p3PEGMAN in various environments, and (d) spectra of p4PEGMAN in various environments.

liquid environment (favorable for sonogel hybrid preparation). Figures 6(b)–(d) show the comparative Raman spectra of the THF solutions, PR-sonogel and some derived bulk hybrids: pMDR1, p3PEGMAN and p4PEGMAN. In the latter cases, highly loaded bulk hybrid samples with OH-TEOS:D-D relations in the ratio of 1.0:1.0 and 1.2:0.8 ml were chosen for adequate Raman measurements. In general, the bulk hybrids exhibit similar Raman signals as in their respective THF solutions, but with a considerably lower intensity: for all polymer-based solutions or bulk hybrids, high intensity bands at 1120 cm^{-1} due to stretching of the C–N bonds and to asymmetric stretching of the C–O–C groups can be observed; at 1338 cm^{-1} a small band due to symmetric stretching of the NO_2 group is shown. On the other hand, within the 1370–1470 cm^{-1} interval, stretching vibrations corresponding to the –N=N– azobenzene bonds are clearly detectable, whereas at ∼1590 cm^{-1} a strong band due to the benzene C=C double bond can be recognized [24]. As shown in figures 6(b)–(d), the reference sonogel does not exhibit any significant Raman signals; thus the observed bands correspond to the functional molecular groups of the dopant species only[5].

It is important to point out that neither FTIR analysis nor Raman spectra gave any definitive evidence of molecular binding involving the SiO_2 host matrix and the functionalized polymers. An explanation of this behavior is due to the lower amount of dopants used in the hybrid sonogel synthesis compared to that of the main inorganic network. Thus, the observed XRD band shifts are mainly produced by the conformational structural changes suffered by the amorphous network as the dopants are embedded.

The optical properties of the p*n*PEGMAN and pMDR1 polymers were studied in THF solution and sonogel phase by UV–vis spectroscopy and the corresponding absorption spectra are shown in figures 7(a) and (b), respectively. Table 2 summarizes some of the optical properties of all polymers in various environments and formats.

As observed in figure 7(a), all azo-polymers in unsaturated THF solutions exhibited a maximum absorption band in the range between 467 and 471 nm due to the π–π^* and n–π^* transitions of the azobenzene group [9]. In this case, since p*n*PEGMAN polymers contain amino–nitro-substituted azobenzene moieties in their structure, they exhibit a total overlap of the π–π and n–π^* bands in their absorption spectra, so that only one absorption band can be observed. This behavior is typical for donor–acceptor substituted azobenzenes, which belong to the 'pseudostilbenes' category according to the Rau classification [6]. On the other hand, p2PEGMAN and p3PEGMAN exhibited a discrete redshifted shoulder, which reveals the presence of traces of intermolecular J-aggregates (head to tail) for these polymers in solution [9]. The presence of aggregates is indicative of possible intramolecular interactions between azobenzene groups. This phenomenon is more evident in the solid state phase since highly polar donor–acceptor substituted azobenzenes have a natural tendency to form pairs in order to reach electronic stability. In most of the cases, the donor group (amine) interacts with the acceptor group (nitro) of the neighbor azobenzene; this behavior was previously reported for other azo-polymers [25]. It is observed from figure 7(b) that, due to its high purity level, the absorption spectra of

[5] Concerning the Raman analysis of the SiO_2 sonogels, it has been observed that these materials present significant Raman emission bands after a thermal treatment of at least 800 °C only [13].

Table 2. Optical absorption properties of the p*n*PEGMAN polymers and pMDR1 in THF solutions, thin film and sonogel formats.

Compound	λ_{max} (nm) THF solution	λ_{max} (nm) thin film	λ_{max} (nm) sonogel	λ_{em} (nm)[a] sonogel	λ_{em} (nm)[b] sonogel
pMDR1	464	477	487	435 625	631
p2PEGMAN	467	488	489	435 625	632
p3PEGMAN	470	452	485	435 625	621
p4PEGMAN	471	417[c] 483	481	435 625	625
p6PEGMAN	467	475	494	435 625	624

[a] Excitation at $\lambda = 200$ nm. [b] Excitation at $\lambda = 500$ nm.
[c] Band due to the presence of H-aggregates.

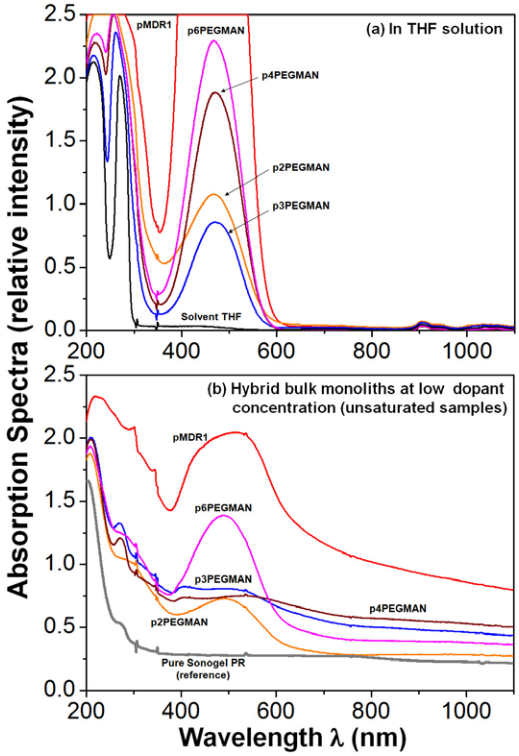

Figure 7. Comparative UV–vis absorption spectra of the pMDR1 and p*n*PEGMAN polymers in THF solution (0.14 mg ml^{-1}) and solid state sonogel phases (1.90:0.02 ml): (a) polymers in THF solutions, (b) pMDR1 and p*n*PEGMAN bulk-based composites.

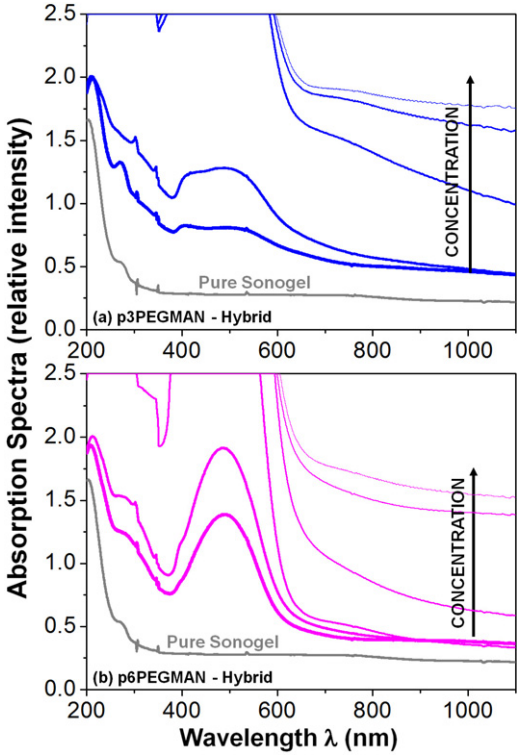

Figure 8. Comparative UV–vis absorption spectra of selected samples with increasing doping concentrations: (a) p3PEGMAN-based composites at: 2.0:0.0 (reference glass), 1.90:0.02, 1.90:0.05, 1.5:0.5, 1.4:0.6 and 1.0:1.0 ml, and (b) p6PEGMAN-based composites at: 2.0:0.0 (reference glass), 1.90:0.02, 1.90:0.05, 1.8:0.2, 1.6:0.4, 1.4:0.6 and 1.2:0.8 ml.

a reference sonogel sample (2.0:0.0) show small absorption bands within the 200–300 nm UV spectral range only. These bands are significantly less intense than those observed for the doped composites and represent typical features of SiO_2-based glassy materials. Thus, it can be ensured that the absorption bands observed for the hybrid composites are mainly due to the organic part and the sonogel matrix does not appreciably contribute to the absorption spectrum of the hybrids due to its impurity-free state. Since in the solid state the molecular concentration is higher, extremely lightly doped samples (1.90:0.02 ml) were selected for absorption experiments in this phase, in such a way that the Beer–Lambert law applies for these partially transparent monoliths; hence analysis of the electronic spectra and absorption properties of the different hybrids is guaranteed.

As an illustration of the controllable conditions feasible for the growing process of the bulk hybrids, figures 8(a) and (b) show a set of examples (for p3PEGMAN and p6PEGMAN-based hybrids, respectively), demonstrating that, for increasing doping concentrations, the relative absorption intensity of the hybrids accordingly increases (samples thickness: ∼0.8 mm). In fact, this procedure ensures controllable increments of the

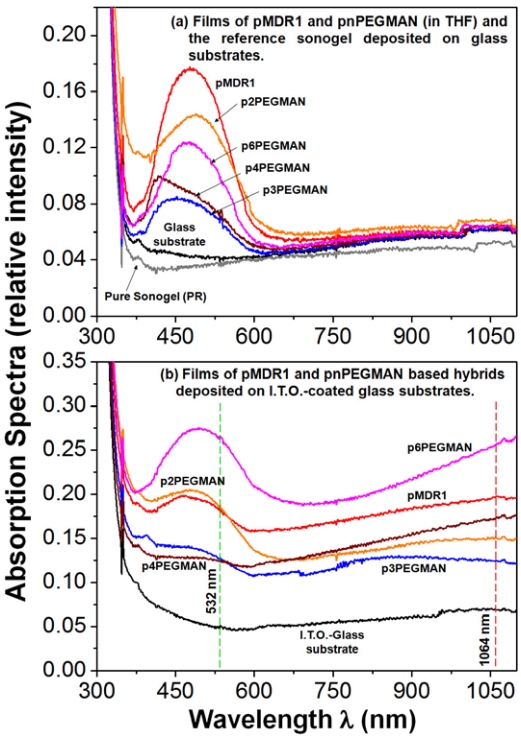

Figure 9. Comparative UV–vis absorption spectra of the p*n*PEGMAN polymers, pMDR1 and pure sonogel-based thin films deposited by spin-coating on: (a) glass substrates from doped THF solutions (∼3–2 mg ml^{-1}) and (b) on glass substrates covered by an ITO electrode thin film. Depositions were performed in this case from the hybrid precursor sols (doped OH-TEOS solution at 50:50% concentration of OH-TEOS:D-D).

molecular loading within the sonogel network, which is crucial for several optical and photonic applications. Typical features of the respective organic molecular systems in solution and in the sonogel solid phase can be observed in these examples, indicating that the electronic states in the solid state are largely determined by those of isolated molecules.

Absorption spectra of the pMDR1 and p*n*PEGMAN polymer films deposited from THF solutions and doped sols on glass and ITO substrates are shown in figures 9(a) and (b), respectively. Deposition of clean THF-based polymer solutions on glass substrates were first performed as an initial test in order to investigate adhesion effects and film homogeneity on the substrates for both the pure sonogel (sol phase) and the polymers in solution (figure 9(a)). In this case, no strict control of the solution concentrations was taken into account (∼3–2 mg ml^{-1}) which explains discrepancies of the relative absorption intensities found for the bulk samples and the hybrid films (see figures 7(b) and 9(b)). As shown in figure 9(a), the azo-polymers showed maxima absorption wavelengths at pMDR1 (λ_{max} = 477 nm), p2PEGMAN (λ_{max} = 488 nm), p3PEGMAN (λ_{max} = 452 nm), p4PEGMAN (λ = 417 nm, λ_{max} = 483 nm) and p6PEGMAN (λ_{max} = 475 nm). Except for p3PEGMAN, all p*n*PEGMAN polymers showed redshifted λ_{max} values, compared to those observed in THF solution, followed by the presence of redshifted discrete shoulders, which can be due to the presence of traces of J-aggregates of the azobenzene chromophores. In particular, the absorption spectrum of p4PEGMAN shows an intense additional blueshifted band at λ = 417 nm, which clearly indicates the presence of antiparallel H-aggregates in this polymer film. A similar behavior was also observed for some azo-polymers of the pnMAN series [5]. On the other hand, pMDR1 exhibited a symmetric absorption band (at λ_{max} = 477 nm) in the same environment.

In contrast, the absorption spectra of the p*n*PEGMAN polymers and pMDR1 in the sol–gel phase deposited on glass substrates covered by ITO (figure 9(b)) exhibit broad absorption bands between 481 and 494 nm and no additional bands and shoulders are observed. Since in this case the dopant polymers are dispersed in a sol–gel environment, the molecules do not show strong intermolecular interactions as they do in the solid state, where they are present in bulk. In the case of the sol–gel films doped with p2PEGMAN and p6PEGMAN the absorption bands were more redshifted compared to those of the other hybrid films of the series; this can be attributed again to the presence of traces of J-aggregates. A similar behavior was observed in the series of grafted polymers bearing RED-PEG dyes (AC-g-PE-RED-PEG), which are precursors of the p*n*PEGMAN polymers [9]. The hybrid film samples, as mentioned before, were also studied under strong IR-laser irradiation in order to investigate the possibility of inducing quadratic NLO–SHG properties in electrically poled hybrid films. In this context, the available laser excitation line (at $\lambda\omega$ = 1064 nm) and the line at the SHG wavelength ($\lambda_{2\omega}$ = 532 nm) are also shown in figure 9(b). The thickness of these films was estimated by AFM to be within the 0.200–0.350 μm range according to the step method: results are summarized in table 3.

Complementary comparative spectroscopic photoluminescence studies were also performed in the p*n*PEGMAN and pMDR1 bulk sonogel hybrids (for lightly doped samples: 1.90:0.05 ml), respectively; as is shown in figures 10(a) and (b). The PL spectra (not normalized, at λ_{ex} = 200 and 500 nm) of the hybrid materials show a strong emission of the pure catalyst-free sonogel, indicating low bulk self-absorption effects and a high optical and chemical purity for this kind of glasses. The features of the PL spectrum for the reference sample have been discussed elsewhere in relation to its precursor reactants [11]. It has been noted in these studies that the reference sonogel exhibits a large PL emission within the 300–600 nm region, comparable to that of highly transparent SiO_2 glasses; this study also explains the two bands observed at 396 and 430 nm. On the other hand, the emission spectra of the hybrid materials, with excitation at λ = 200 nm (figure 10(a)) exhibit a weak emission band with a broad vibronic structure centered at λ = 435 nm followed by a middle intensity band at λ_{max} = 625 nm (a strong intensity band has a value of the order of 10^7 or more a.u.). Azobenzenes bearing nitro groups usually do not fluoresce when they are excited at λ_{max}. However, in the case of the hybrid materials, we can observe a moderate emission, with excitation at λ = 200 nm. Since the fluorescence spectra of the pure sonogel is highly fluorescent, showing an intense emission at λ = 435 nm, we can conclude that all the emission comes from the sonogel matrix and is partially quenched by the doping p*n*PEGMAN polymers, which

Table 3. Linear optical refractive indices of the pMDR1 and p*n*PEGMAN polymer-based hybrids in bulk (at $\lambda = 632$ nm) and hybrid thin films (at $\lambda = 532$ nm). Measurements of the film thicknesses are also reported.

Hybrid samples (bulk or thin film format)	Refractive index: n_{Bulk}	Refractive index: n_{Film}	Thickness d_{Film} (by AFM, nm)	Thickness d_{Film} (by transm. spectra, nm)
Pure sonogel (PR)	1.394	—	—	—
ITO-Substrate	—	1.554	—	—
pMDR1	1.425	1.561	318	355.32
p2PEGMAN	1.492	1.556	329	428.51
p3PEGMAN	1.832	1.584	293	310
p4PEGMAN	1.425	1.405	360	317.00
p6PEGMAN	1.662	1.600	214	210.81

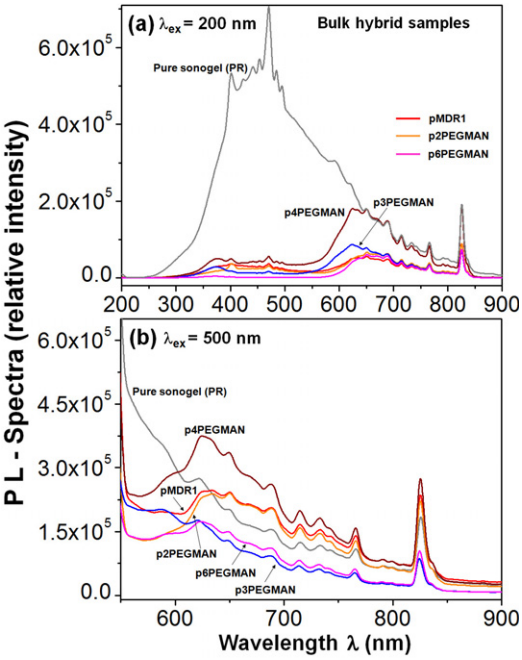

Figure 10. Comparative PL spectra obtained from the solid state sonogel phase in pure and lightly doped samples (2.0:0.0 and 1.90:0.05 ML, respectively): (a) excitation wavelength at $\lambda_{\text{ex}} = 200$ nm and (b) excitation wavelength at $\lambda_{\text{ex}} = 500$ nm.

precisely absorb within this region. It is very well known that the nitro and azo groups usually act as fluorescence quenchers. Nevertheless, when the emission spectra of these hybrid materials are recorded at $\lambda_{\text{ex}} = 500$ nm, very different fluorescence spectra are obtained (figure 10(b)). In this case, a low intensity broad emission band is observed around $\lambda = 623$–631 nm for the whole series of hybrid materials. Although azobenzenes are usually fluorescence quenchers, in these hybrid materials they can be complexed by TEOS, so that the p*n*PEGMAN polymers can give rise to moderate emission in this environment.

The estimated values of the linear refractive index for the bulk hybrid and film composites (n_{Bulk} and n_{Film}, respectively) are shown in table 3. In general, the refractive index in thin films is lower than that of the corresponding bulk materials; this decrease is a direct consequence of the density reduction provoked by the presence of organic solvent agents during the deposition process, porous reconfiguration in the thin film structure and the interface electronic influence, which is more significant for thin films due to the lower dimensions [26, 27]. According to the Brewster angle method, the p3PEGMAN polymer-based bulk hybrid presents the maximum n_{Bulk} refractive index, whereas p4PEGMAN and pMDR1 exhibit similar n_{Bulk} values. As expected, the pure reference sonogel shows the minimum n_{Bulk} value due to the high porosity of the network containing air within its constituting nanopores, making the n_{Bulk} value closer to unity. On the other hand, a vast number of cavities within the hybrid systems are filled up with the guest polymers, increasing their respective refractive indices. In thin film samples, the n_{Film} values obtained from the transmission spectra analysis according to the envelope method show a maximum refractive index for the p6PEGMAN sample; the pMDR1 and p2PEGMAN film samples exhibit larger refractive indices than those of their respective bulk hybrids, a possible explanation for these particular cases is the fact that, within these hybrid film networks, a minor number of empty cavities/pores are present due to the relatively higher implemented doping concentrations (50/50%) which increase their n_{Film} values. The film thicknesses measured by the two implemented methodologies are also listed in table 3, and d_{Film}-values of the order of 200–380 nm have been obtained for the studied samples. Coherent results with no major discrepancies show the accuracy and convenience of implementing both methodologies in combination.

Finally, the hybrid film samples deposited on ITO substrates were tested as candidates for quadratic NLO applications via the standard SHG technique. This procedure was carried out after performing the molecular orientation of the guest polymers via a corona-poling system at adequate temperatures for each sample (above the T_{g} values). The poling method influences the macroscopic second-order polarization component through the amount of long-range and long-term order that is imposed on the system. The orientation of the molecular dipoles can be described by an order parameter Φ as explained below. In this way, the structural centrosymmetric organization within the amorphous hybrid films can be broken, leading to a polar order induced by the electrically oriented polymers. This (ferroelectric) polar order is equivalent to a non-centrosymmetric arrangement which is a fully required condition for the observation of quadratic $\chi^{(2)}$-NLO effects [20–22]. In fact, as shown in figures 11(a) and (b), the comparative absorption spectra obtained before and after performing the electrical poling procedure of the samples (two representative spectra for pMDR1 and p2PEGMAN are

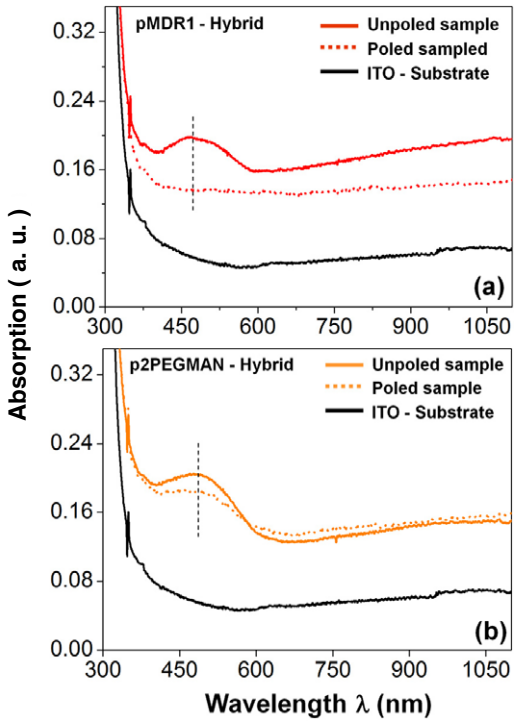

Figure 11. Comparative absorption spectra obtained before and after performing electrical poling on selected film samples, case of: (a) pMDR1-based hybrid film and (b) p2PEGMAN-based hybrid film.

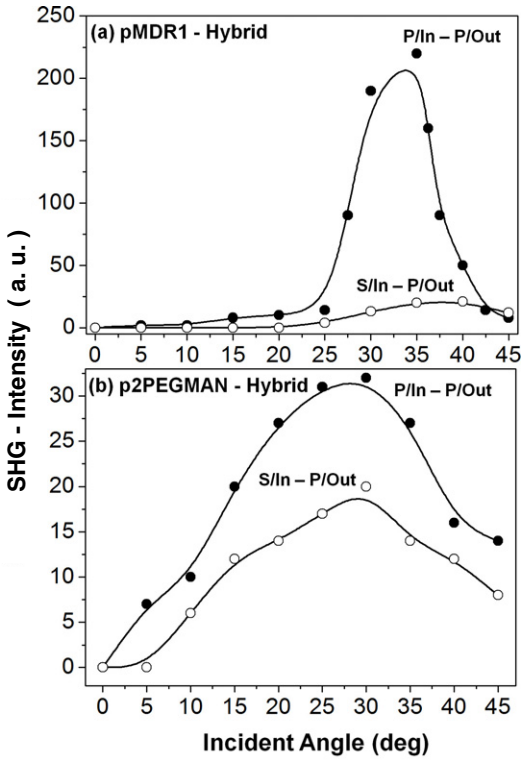

Figure 12. Angle-dependent SHG measurements in P/In-P/Out and S/In-P/Out polarizing configurations, case of: (a) pDR1-based hybrid film and (b) p2PEGMAN-based hybrid film. The continuous lines serve only as a visual guide in order to follow the SHG tendency in dependence with the incident angle.

shown) exhibit a drastic change on the absorptive properties of the hybrid films: immediately after poling a decrease in absorbance (hypochromic shift) at λ_{MAX}, as well as a slight shift toward longer wavelengths (bathochromic), can be observed. The electrostatic field aligns the dipoles in the direction of the poling field, leading to a change in the intensity of the absorption spectrum, i.e. to dichroism [28, 29]. This orientation is maintained, depending on the T_g values, by the polymer within the host matrix as the temperature is lowered. The permanent part of the hypochromic shift observed after poling is mainly attributed to the permanent alignment of the chromophores in the polymer host.

The analysis of the absorption spectra allows the evaluation of the orientational order, which can be defined in practical terms as [28, 29]: $\Phi = 1 - (\frac{A_2(\lambda_{MAX})}{A_1(\lambda_{MAX})})$, where $0 \leqslant \Phi \leqslant 1$, $A_1(\lambda_{MAX})$ and $A_2(\lambda_{MAX})$ are the sample absorption before and after electrical poling at λ_{MAX}, respectively. Table 4 summarizes the Φ parameters evaluated for the studied samples; due to the low T_g values of the available implemented polymers (see table 1), these parameters are rather low compared to other azo-polymer poled films [28, 30]. As for deposition parameters, the relation between microstructure, NLO and optoelectronic properties of the obtained films needs to be further understood and clarified since the magnitude of the Φ parameters does not correspond to the T_g values, indicating the doping and poling procedure in our sonogel process is still ineffective and needs to be further improved. However, under the scope of this paper, the feasibility of the poled sonogel hybrid films to exhibit quadratic NLO effects

Table 4. Orientational order (Φ values) and effective quadratic NLO properties ($\chi^{(2)}_{eff}$ values) of the pMDR1 and p*n*PEGMAN polymer-based hybrid films.

Hybrid film samples	Order parameter $\Phi = 1 - (\frac{A_2(\lambda_{MAX})}{A_1(\lambda_{MAX})})$	$\chi^{(2)-(P-P)}_{eff_{Hybrid-Film}}$-coefficients (pm V^{-1})
pMRD1	0.32	0.230
p2PEGMAN	0.15	0.160
p3PEGMAN	0.13	0.012
p4PEGMAN	0.09	—
p6PEGMAN	0.07	—

is demonstrated in figures 12(a) and (b) by discrete angle-dependent SHG experiments.

Figures 12(a) and (b) reveal non-negligible and stable SHG signals for the poled pMDR1 and p2PEGMAN-based hybrid films, showing typical Maker fringes with a minima at 0° and a maxima within the 25°–40° range which are characteristic of poled organic films. In fact, stronger P/In-P/Out SHG signals can be observed and are indicative of enhanced phase-matching conditions (better molecular laser excitation along the long chromophore axes or $\chi^{(2)}_{33}$ direction) in the aligned films [20–22]. SHG signals were surprisingly stable for the reference pMDR1-based hybrid film sample through the lower T_g value of the constituting guest molecule; likewise stable NLO signals were obtained for the p*n*PEGMAN ($n = 2, 3$) samples with higher T_g values,

whereas for the $n = 4$ and 6 samples the extremely weak and unstable SHG signals rapidly vanished with laser irradiation, even when the corresponding T_g values are slightly above the ambient temperature. According to the relative Maker-fringes method, an estimated value of the second-order effective NLO susceptibility or $\chi^{(2)}_{\text{eff}}$ coefficient was evaluated. To this end, a quartz reference crystal was used to calibrate the SHG experimental set-up, providing, according to the following equation, the estimated $\chi^{(2)}_{\text{eff}_{\text{Hybrid-Film}}}$ values:

$$\chi^{(2)-(\text{P}-\text{P}),(\text{S}-\text{P})}_{\text{eff}_{\text{Hybrid-Film}}} \propto \chi^{(2)-\text{Quartz}-\text{Cr}}_{11} \times \left(\frac{2l_c^{\text{Quartz}-\text{Cr}}}{\pi l_{\text{Film}}}\right)\left[\frac{I_{2\omega}^{\text{Film}^{\text{MAX}}}}{I_{2\omega}^{\text{Quartz}-\text{Cr}^{\text{MAX}}}}\right]^{1/2}, \quad (5)$$

where l_{Film} is the film thickness, $l_c^{\text{Quartz}-\text{Cr}} \approx 21\ \mu$m is the coherence length of the quartz reference crystal and $\chi^{(2)-\text{Quartz}-\text{Cr}}_{11} \approx 1.2\ \text{pm V}^{-1}$ is its respective NLO coefficient [31]. $I_{2\omega}^{\text{Quartz}-\text{Cr}^{\text{MAX}}}$ and $I_{2\omega}^{\text{Film}^{\text{MAX}}}$ are the SHG intensities at maximum of the Maker fringes observed for the reference crystal and the film sample, respectively. In table 4 the representative $\chi^{(2)-(\text{P}-\text{P})}_{\text{eff}_{\text{Hybrid-Film}}}$ coefficients, evaluated according to the last simplified formula for the samples displaying stable SHG signals, are also listed. The $\chi^{(2)}_{\text{eff}}$ values are rather small compared to those of the reference crystal and other similar organic materials, which are in the range of 1–30 pm V^{-1} [32][6].

Although the implemented polymers strongly absorb within the spectral region of the SHG (see figure 9), the $\chi^{(2)}_{\text{eff}}$ values are quite small indicating poor alignment (mainly due to the low T_g values, as mentioned before), and collaterally, poor molecular interactions between the dopant species and the host matrix (via covalent bonding) which would lead to an appreciable enhancement of the SHG effect. As a next step of this investigation, other functionalized push–pull azo-polymers with considerably higher T_g values are being investigated within the hybrid sonogel environment, pointing to nonlinear waveguiding applications and quasi-phase-matching (QPM) effects. Here the chromophore–chromophore electrostatic interactions and aggregation effects, which also play an important role in the observation of quadratic NLO phenomena, should be carefully taken into account. Indeed, the rigidity of the sonogel environment confines the molecules to narrower spaces, thereby restraining their mobility and favoring interactions between molecular groups at shorter distances. These investigations are currently underway and will be presented in a second part of this contribution.

4. Conclusions

The highly pure SiO_2 sol–gel network obtained by sonochemical reactions behaves as an appropriate host for organic azo-compounds. Large surface areas and nanoporosity obtained at room temperature, together with the stable mechanical performance achieved after drying, provide an excellent environment for the confinement of the organic chromophores in rigid doped glasses with convenient geometrical shapes, pointing to potential, low-cost optoelectronic applications. The p*n*PEGMAN and pMDR1 azo-polymers were successfully introduced within the amorphous SiO_2 network as demonstrated by several spectroscopic and structural techniques. The control on doping concentration and malleability of the sol suspensions allowed easy preparation of both bulk geometrical hybrid monoliths and hybrid thin film samples with good structural and mechanical properties suitable for optical and morphological characterizations. In fact, the wide, high transmission window displayed by the host matrix within the whole UV–vis spectral range permits an optimal tuning of the electronic properties of the guest molecular systems in the solid state, which is a key point towards the development of novel π-conjugated composites, i.e. the absorption spectra of the hybrids indicates that the electronic states in the solid state are largely determined by those of isolated molecules.

Raman, FTIR and PL techniques have not shown any evidence of strong molecular interactions between the host SiO_2 network and the guest organic compounds. Indeed, only significant spectroscopic bands owing to the functional groups of the embedded chromophores or the host matrix were separately detected. On the other hand, the sonogel hybrid film samples deposited on ITO substrates were able to be electrically oriented, giving rise to non-centrosymmetric polar arrangements suitable for quadratic NLO characterizations. Since the SHG signals were quite small due to poor orientational order, again, no evidence of strong bonding effects between the dopant species and the sonicated SiO_2 network, strengthening the alignment process, was found. Thus, the high purity level displayed by the sonogel network and the poor interactions occurring within the guest–host system with these kinds of functionalized compounds ensure optimal optical characterizations to evaluate several photophysical properties of the organic part of these composites, preserving the pristine optical properties of the guest molecules. Under this scope, in order to further explore NLO and solid state applications with these kinds of interesting hybrid materials, the development of novel SiO_2-based hybrid sonogel composites with thermally improved azo-polymers is currently underway.

[6] Due to the experimental difficulties and bad definition of the obtained Maker fringes, the evaluation of the tensorial $\chi^{(2)}_{ij}$ components of the nonlinear susceptibility was not performed by theoretical fittings.

Acknowledgments

We are grateful to Dr Ma Esther Mata-Zamora, Mr Hugo Sanchez-Flores (CCADET-UNAM) and Mrs Leticia Baños (IIM-UNAM) for their valuable support in recording Raman, FTIR and XRD spectra, respectively. We also wish to thank Dr Neil Bruce for English revision of the manuscript. This work was supported by projects SEP-CONACyT (grant U-49846F) and PAPIIT-DGAPA (grant IN-101207).

References

[1] Natansohn A and Rochon P 2002 Photoinduced motions in azo-containing polymers *Chem. Rev.* **102** 4139–75
[2] Ichimura K 2000 Photoalignment of liquid-crystal systems *Chem. Rev.* **100** 1847–74

[3] Delaire J A and Nakatani K 2000 Linear and nonlinear optical properties of photochromic molecules and materials *Chem. Rev.* **100** 1817–46
[4] Sourisseau C 2004 Polarization measurements in macro- and micro-Raman spectroscopies: molecular orientations in thin films and azo-dye containing polymer systems *Chem. Rev.* **104** 3851–91
[5] Freiberg S, Lagugné-Labarthet F, Rochon P and Natansohn A 2003 Synthesis characterization of a series of azobenzene-containing side-chain liquid crystalline polymers *Macromolecules* **36** 2680–8
[6] Rau H 1990 *Photochemistry and Photophysics* vol II, ed J K Rabek (Boca Raton, FL: CRC Press)
[7] Shin D M, Schanze K S and Whitten D G 1989 Solubilization sites and orientations in microheterogeneous media. Studies using donor–acceptor-substituted azobenzenes and bichromophoric solvatochromic molecules *J. Am. Chem. Soc.* **111** 8494–501
[8] Garcia T, Morales-Saavedra O G, Carreón-Castro M P and Rivera E 2006 unpublished
[9] Rivera E, Carreón-Castro M P, Salazar R, Huerta G, Becerril C and Rivera L 2007 Preparation and characterization of novel grafted polyethylene based azo-polymers bearing oligo(ethylene glycol) spacers *Polymer* **48** 3420–28
[10] Morales-Saavedra O G, Castañeda R, Ocotlan-Flores J, Román-Moreno C, Ortega-Martínez R and Pelzl G 2008 Chlorine-substituted bent-core LC-based sonogel hybrid materials: synthesis and optical properties *Mol. Cryst. Liq. Cryst.* **488** 56–73
[11] Morales-Saavedra O G, Rivera E, Flores-Flores J O, Castañeda R, Bañuelos J G and Saniger J M 2007 Preparation and optical characterization of catalyst free SiO_2 sonogel hybrid materials *J. Sol–Gel Sci. Technol.* **41** 277–89
[12] Brinker C J and Scherer G W 1990 *Sol–Gel Science: the Physics and Chemistry of Sol–Gel Processing* (New York: Academic)
[13] Flores-Flores J O and Saniger J M 2006 Catalyst-free SiO_2 sonogels *J. Sol–Gel Sci. Technol.* **39** 235–40
[14] Morales-Saavedra O G and Rivera E 2006 Linear and nonlinear optical properties of trans- and cis-poly(1-ethynylpyrene) based sonogel hybrid materials *Polymer* **47** 5330–7
[15] Morales-Saavedra O G, Huerta G, Ortega-Martinéz R and Fomina L 2007 *J. Non-Cryst. Solids* **353** 2557–66
[16] Caricato A P, Fazzi A and Leggieri G 2005 A computer program for determination of thin films thickness and optical constants *Appl. Surf. Sci.* **248** 440–5
[17] Swanepoel R 1983 Determination of the thickness and optical constants of amorphous silicon *J. Phys. E: Sci. Instrum.* **16** 1214–22
[18] Manifacier J C, Gasiot J and Fillard J P 1976 A simple method for the determination of the optical constants n, k and the thickness of a weakly absorbing thin film *J. Phys. E: Sci. Instrum.* **9** 1002–4
[19] Gauthier N 1987 Wavelength dependence of the refractive index *J. Teach. Phys. Edu.* **25** 501–3
[20] Prasad P N and Williams D J 1991 *NLO Effects in Molecules and Polymers* (New York: Wiley) pp 3–7
[21] Nalwa H S and Miyata S (ed) 1997 *Nonlinear Optics of Organic Molecules* (Boca Raton, FL: CRS Press)
[22] Kajzar F and Swalen J D (ed) 1996 *Organic Thin Films for Waveguiding Nonlinear Optics* (San Jose, CA: CRS Press)
[23] Boyd R W 1992 *Nonlinear Optics* (San Diego, CA: Academic) pp 65–7
[24] Socrates G 2004 *Infrared and Raman Characteristic Group Frequencies Tables and Charts* (New York: Wiley)
[25] Iftime G, Lagugné-Labarthet F, Natansohn A and Rochon P 2000 Control of chirality of an azobenzene liquid crystalline polymer with circularly polarized light *J. Am. Chem. Soc.* **122** 12646–50
[26] Krbal M, Wagner T, Kohoutek T, Nemec P, Orava J and Frumar M 2007 The comparison of Ag–As33S67 films prepared by thermal evaporation (TE), spin-coating (SC) and a pulsed laser deposition (PLD) *J. Phys. Chem. Solids* **68-6** 953–7
[27] Pulker H K 1979 Characterization of optical thin films *Appl. Opt.* **18** 1969–77
[28] Mortazavi M A, Knoesen A, Kowel S T, Higgins B G and Dienes A 1989 Second-harmonic generation and absorption studies of polymer-dye films oriented by corona-onset poling at elevated temperatures *J. Opt. Soc. Am.* B **6** 733–41
[29] Yamaoka K and Charney E 1972 Electrical dichroism studies of macromolecules in solutions. I. Theoretical considerations of electric dichroism and electrochromism *J. Am. Chem. Soc.* **94** 8963–74
[30] Perez-Martínez A L, Gómez-Sosa G and Ogawa T 2005 The orientation stability and UV irradiation of poly(hexa2,4diynilene1,6dioxy)benzoates and cinnamates containing disperse Red 19, Journal of Macromolecular Science *Pure Appl. Chem.* **42** 1561–72
[31] Kuzyk M and Dirk C 1998 *Characterization Techniques and Tabulations for Organic Nonlinear Optical Materials* vol 60 (New York: Dekker)
Sutherland R *Handbook of Nonlinear Optics* vol 52 (New York: Dekker)
[32] Singer K D, Kuzyk M G, Holland W R, Sohn J E, Lalama S J, Comizzoli R B, Katz H E and Schilling M L 1988 Electro-optic phase modulation and optical second-harmonic generation in corona-poled polymer films *Appl. Phys. Lett.* **53** 1800–2